DOI: 10.13009/EUCASS2022-4535
9TH EUROPEAN CONFERENCE FOR AERONAUTICS AND SPACE SCIENCES (EUCASS)

# Experimental investigation of the regression rate in an end-burning swirling flow hybrid rocket engine

Tomasz Palacz and Jacek Cieślik
AGH University of Science and Technology
Al. Mickiewicza 30, 30-059 Cracow, Poland
correspondence: palacz@agh.edu.pl

## Abstract

This paper presents preliminary results on the regression rate characterization in the end-burning hybrid rocket engine. The long-term goal is to develop a hybrid propellant thruster as green chemical propulsion for small satellites. The hybrids may offer high performance in a very compact and low complexity system using green and low-cost propellants. The test facility has been developed and a test campaign was performed for a 25 mm chamber diameter end-burning hybrid with GOX/HDPE propellants. The experimental variables were burn duration and oxidizer mass flow rate. Obtained regression rate data confirms non-uniform behavior in end-burning hybrids, but the distribution of the regression rate is the opposite of those reported in previous studies.

## 1. Introduction

### 1.1 Green chemical propulsion for small spacecrafts

In recent years the space industry experiences renewed interest from the public and private players. We observe increased commercial activities on Low Earth Orbit and beyond, as well more long-term exploration plans for deep space, such as Lunar manned missions, asteroid mining, or even Mars colonization. Technology advancements allowed to lower the launch cost to space and bring small satellites to life, which along with fresh business models drives public and private investments into the sector. This led to rapid growth in the number of satellites launched to space.

In the last two years, we have sent more satellites than in the previous 70 years. Most of the launched satellites are in a small class (< 500 kg), from which the most common are nanosatellites (< 10 kg), in the popular CubeSat form factor. The extensive use of small satellites for both exploration and commercial applications drives the need for dedicated propulsion systems, that would be more suited in terms of size, mass, power consumption, safety, and ease of handling. Additionally, the choice of the propulsion system has also restricted the fact that small spacecrafts are usually launched as a piggyback payload, and they shall not pose any risk to the main payload. Currently, there are many electric propulsion technologies developed to meet the need of smallsats, as for most cases, they can offer better performance and cost than chemical propulsion, especially for the smallest of satellites.

However, electric propulsion cannot offer high thrust for fast maneuvers, which need to deliver large $\Delta v$ in a short time, e.g., in case of orbit insertion, satellite deployment, EOL disposal, or CAMs. Recent developments of alternative chemical propellants, which are sought as a replacement for toxic hydrazine also for large satellites, enabled small spacecraft missions to use chemical propulsion (e.g. NASA's Green Propellant Infusion Mission). The two most mature hydrazine replacement propellants, LMP-103S and AF-M315E, are blends of ionic liquids Ammonium Dinitramide (ADN) and Hydroxylammonium Nitrate (HAN), respectively. Both propellants have been verified in a space mission, LMP-103S on Prisma spacecraft [1], and AF-M315E on a GPIM mission [2], and delivered at least equivalent performance to the hydrazine. However, propellants based on these ionic liquids are not entirely green and are often called "reduced toxicity", as they are not environmentally friendly and are toxic to organic tissue. In addition, Whitmore [3], points out several issues with these propellants that make them unsuitable for small spacecraft. Ionic liquids-based propellants must be ignited with the use of catalyst beds that are preheated to more than 340-370 °C, due to high water content, which in turn is required to reduce decomposition risk. This preheat requirement increases the complexity, dry mass, and power consumption of the system, which is highly unfavourable in relation to small spacecrafts. For example, ECAPS 1N LMP-103S thruster requires around 9.25 W of power for roughly 600 – 720 s to read the minimum required temperature, which translated to 5 – 7 kJ of energy input for the startup [4]. For the Prisma

DOI: 10.13009/EUCASS2022-4535



mission, the pre-heat time was 30 minutes, which translates to more than 16 kJ of total energy input for the startup of the single thruster [1].

### 1.2 Hybrid propellant thruster as a viable chemical propulsion alternative

The hybrid rocket engines, or hybrid propellant thruster (a term proposed for hybrid chemical propulsion in case of its use for space to distinguish it from hybrid chemical-electric propulsion), are typically built with solid fuel grain in the combustion chamber and liquid or gaseous oxidizer in the external tank. This separation of propellants gives inherent safety of handling and operations, in comparison to solid rocket motors, while a single propellant in the liquid phase requires a much less complicated hydraulic feed system than in the liquid bipropellants, making hybrid propellant thruster (HPT) relatively simple in terms of mechanical design. At the same time, hybrids can achieve performance (in terms of specific impulse) in the range between solid propellants and bipropellants, Additionally, HPTs can be thrust throttled and shut down, or even restarted. All these advantages suggest that hybrid propulsion is a good candidate for spacecrafts as it may offer benefits in terms of cost, complexity, reliability, and performance.

In comparison to mentioned reduced toxicity chemical propulsion, HPT can work with stable and safe propellants, which are extremely low cost and common (industry grade), for example, nitrous oxide or GOX as an oxidizer and HDPE (High-Density Polyethylene) as fuel. Most fuels are inert, while considered oxidizers are well-known, safe to handle, and compatible with most materials. In terms of performance, it can provide specific impulses comparable to state-of-the-art non-cryogenic bipropellants (> 300 s), which is over 30% better than ADN or HAN-based monopropellants. What is more, HPT propellants are storable in a wide range of temperatures, while reduced toxicity propellants require to be kept above 0°C, as they may freeze or precipitate.

Most of the work done with hybrids is for large-scale applications such as sounding rockets and small launch vehicles. More recent studies consider using HPT as a space thruster for various missions like orbit injection for the geostationary satellite [5], deep space exploration [6], [7], or in-situ Mars ascent vehicle [8]. Such a trend is justified by the market need for green and low-cost propulsion alternatives. As of 2022, the single commercial application of hybrid rocket engines is Virgin Galactic's rocket-powered aircraft to provide suborbital spaceflight to space tourists, although there are other endeavors to develop and operate hybrid-propellant micro launchers. To date, however, no HPT has been used for in-space propulsion.

### 1.3 Recent developments of hybrids for in-space applications

Recently, there have been several important developments on the path to increasing the technology readiness level of the hybrid propellant thruster to a flight-ready level. Whitmore et al. [9] have developed a green, restartable hybrid thruster with a size that applies to a wide range of small spacecrafts. The 22N thruster uses 3D printed ABS and GOX as propellants, with a novel arc ignition method [10]. JPL develops a hybrid propellant thruster for CubeSats that could fit within a 12 U envelope and deliver $\Delta v$ of over 200 m/s to a 25 kg spacecraft [11]. The 40N thruster uses GOX/PMMA and augmented GOX/methane spark igniter. It has been successfully tested in vacuum conditions with multiple reignitions, providing more than 300 s of specific impulse [12]. NASA Ames has performed a series of tests on the 25N hybrid for small spacecrafts developed over several years [13]. Their thruster uses N2O/PMMA and N2O/ethylene augmented spark ignitor.

The above designs use a conventional hybrid propellant thruster configuration, in which fuel grain is cylindrical with a central port. The port may have different cross-sections, usually to enhance the regression rate. Cylindrical configuration results in a high length to diameter ratio, which is not desirable for in-space propulsion due to volume restrictions. Moreover, during the burn the fuel mass flux changes due to expanding fuel port diameter and fuel surface area exposed to the combustion. It leads to an O/F shift, which affects the performance, thus it may not be constant throughout the entire burn. Although the O/F shift may have a negligible impact on the performance in some designs [14], for in-space propulsion, it may be important to deliver reliable and constant impulses.

Constant performance and thrust without O/F shift can be achieved, in theory, by keeping fuel surface area constant. The fuel grain may be in form of a cylinder without any port and with only the face surface exposed for the combustion. Provided that oxidizer mass flow is constant, this should result in a constant fuel regression rate without any changes to the fuel surface area during the burn. Such hybrids are called end-burning (EBH), and in comparison to the conventional configuration, in addition to the constant performance, they may offer better volume and mass utilization due to the small length to diameter ratio of the combustion chamber. In general, however, end-burning hybrids are much less studied, and further work is needed to better assess their benefits and drawbacks.

Of particular importance is the regression rate behavior concerning various design parameters, such as chamber diameter, injection geometry, and oxidizer mass flux. While for conventional hybrids, the internal ballistics are well studied, allowing for the predictable design, there is limited data for the end-burning configuration. Usually, in EBH, the oxidizer is injected tangentially (so-called swirling injection) forming a vortex flow field with the axis

DOI: 10.13009/EUCASS2022-4535

orthogonal to the fuel grain surface. Such conditions are principally different from those present in the conventional hybrids, which suggests that EBH may require alternative design rules and variables to be considered for successful design and operation.

Rice et al. [15] have first developed the concept of the end-burning hybrid, and tried to determine the effects of combustion chamber diameter, injected oxygen mass velocity, and distance between the injection point and fuel grain surface on the axial regression rate. Post-test observation of the fuel surface suggested that the flow-field in the chamber of this diameter (10 cm) and tangentially injected oxidizer consists of two interwound spirals, inner and outer. For GOX/HTPB propellants they derived axial regression rate:

$$\dot{r}_{ax} = G_{ox}^{0.62}(3.32 + 0.0347\, G_{inj} - 0.224\, D_{inj}), \quad \textbf{(1)}$$

where $\dot{r}_{ax}$ – regression rate in the axial direction (mm/s), $G_{ox}$ – oxidizer mass flux (g/cm2-s), $G_{inj}$ – injector port mass flux (g/cm2-s), $D_{inj}$ – distance from the injection point to the fuel surface.

More recently, the end-burning swirling flow hybrid has been studied by Hayashi et al. [16]. Only a few experiments have been performed, and little data is available. The authors expressed the regression rate of the GOX/paraffin in the axial direction and compared it with experimentally obtained data. They have noticed significant regression rate non-uniformity in the radial direction and explained them by the radial distribution of the heat coefficient at the face surface of the fuel derived by Volchkov et al. [17]. However, they have not provided more information on the non-uniformity or the effect of the injector design on the flow field. The group from SPLab of Politecnico do Milano has been extensively working with the “vortex flow pancake” hybrid [18]. Their configuration included two flat fuel grains with free space in between serving as a combustion chamber with a tangentially injected oxidizer. In this design both grains are end-burning. They used GOX as an oxidizer and paraffin-SEBS (60-40%) or HTPB as a fuel. They have performed a CFD analysis, cold flow visualization with a tracer, and hot-fire testing. They estimated the average regression rate in the axial direction but noticed non-uniformities and patterning along the radial direction, as well as a significant disproportion between the upper and lower fuel grains [19], [20]. The EU project called HYPROGEO aimed to develop a constant thrust hybrid compatible with a long burn duration (250N, 5000 s) [5]. The design used an end-burning, swirling flow concept with 98% HTP/HTPB propellants. The authors applied a small distance between the injection point to the fuel surface and used a passive actuator to compensate for the fuel regression. The hot-fire testing included different oxidizer mass flow rates and the number of injectors. The radial distribution of the regression rate is axisymmetric but is far from uniform, which seems to be the same as reported by Hayashi at el. [16]. By using more injectors, researchers have obtained more uniform radial regression rate. Still, the non-uniformities were present with higher regression rate in the central area of the fuel surface, and it seems to influenced the OF ratio shift [21].

This paper reports the first results of the hybrid propellant thruster study at the AGH University of Science and Technology in Poland. The goal is to experimentally investigate the axial and radial regression rate in end-burning hybrid for different design variables, as the available literature does not provide consistent information. In general, the motivation behind work at AGH is to design, develop, and test hybrid as a green, chemical propulsion system for small spacecrafts.

## 2. Experimental setup

### 2.1 Test Stand

A new test facility has been developed as part of the research on the hybrid propellant thrusters being done at the AGH. It consists of the test article (thruster model), feed system, and data acquisition & control system. The test stand is capable of handling hot-fire testing of up to 50 N. Currently, the feed system can operate with GOX up to 10 bar. The measurements include pressures in different points of the feed system and the thruster, temperatures using thermocouples, mass flow rate, and thrust using a baffle plate. The mass flow rate of the oxidizer is controlled by the manual setting of the output pressure from the regulator.

The feed system, schematically shown in Figure 1, consists of two pressure lines – for GOX and nitrogen gas. Each line is built with 12 mm stainless steel tubing, solenoid valves (Bürkert type 6213), and check valves to isolate the pressure tanks from the system. In the oxygen line, an additional manually switched solenoid valve and a second check valve is installed for safety. Two lines join into one line with a mass flow meter (Bronkhorst D-6360A, 5-250 ln/min O2, accuracy ± 1,0 % RD plus ± 0.5% FS), from which the smaller tubing (6 mm) connects to the thruster. The pressure is measured using a 0 – 100 bar WIKA transducer with accuracy ± 2% FS. The custom DAQ and control system allows for up to 24-bit, 4.8kHz measurements, as well as actuator operation up to 24 V. The test stand is remotely controlled via custom PC software and Ethernet interface, allowing for wired and wireless communication.

DOI: 10.13009/EUCASS2022-4535



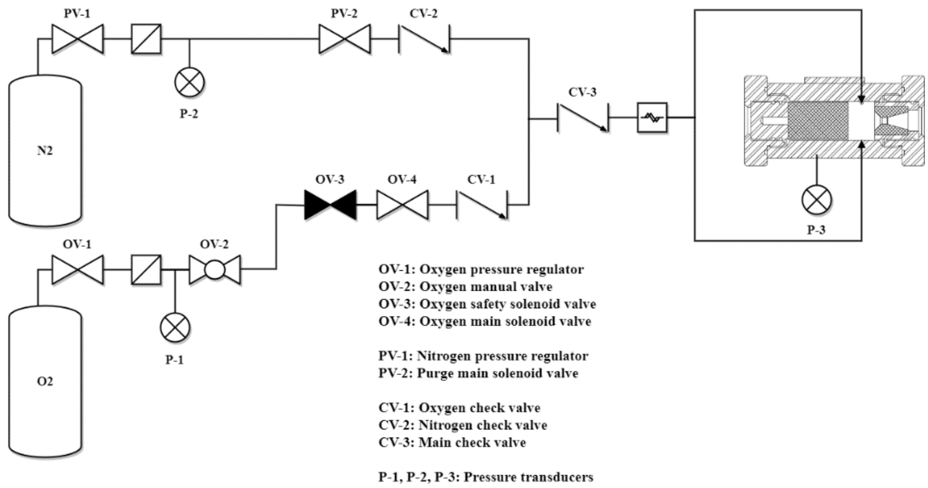


Figure 1. The P&ID diagram of the feed system.

## 2.2 Thruster Test Article

The thruster test article has been designed to be modular, easy to handle and allow fast replacement of the fuel grain. It has a central square body and two cylindrical end caps. The end caps are mounted to the central body by the M36x2 thread, which allows quick assembly. The end caps contain the nozzle and the bulkhead. The nozzle is built in two pieces – a graphite nozzle insert and a nozzle insulator made of cotton - phenolic resin composite, which is sealed with an O-ring. The bulkhead is a simple cylinder with an O-ring seal and a threaded hole for fuel grain attachment. The central body, both end caps, and bulkhead are made of stainless steel. The cross-section of the thruster is shown in Figure 2.

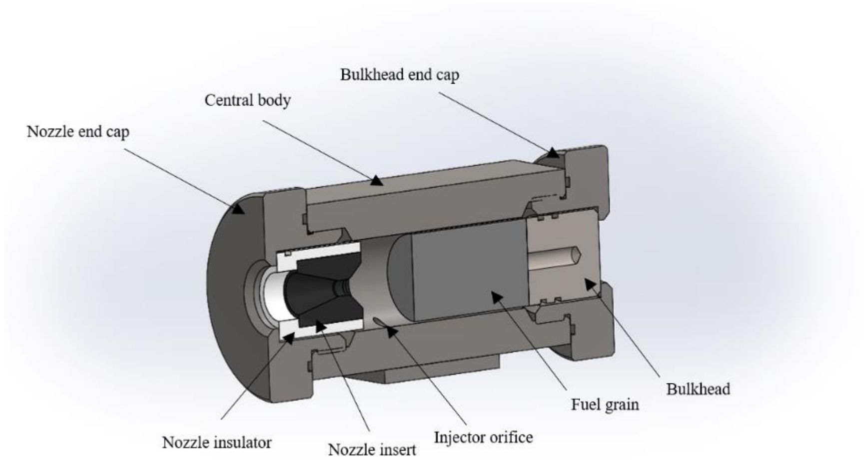


Figure 2. Section view of the thruster test article

The thruster has a 25 mm combustion chamber diameter, 4.5 mm nozzle throat diameter with a 12 mm exit diameter, and a typical 15° divergent half-angle. The oxidizer is injected tangentially by two 1.5 mm orifices approximately 8 mm from the nozzle. The initial distance from the injection point to the fuel surface is controlled by changing the length of the fuel grain. The fuel grain has a tapped hole on the aft end, which is used to mount the grain to the bulkhead with the double-sided threaded pin, to keep it in place during the burn. The thruster can accommodate injection distance up to 38 mm, which corresponds to fuel grain length between 10 and 48 mm, and combustion chamber length of 10 mm to 47 mm. For this study, HDPE fuel grains with a length of 40 mm have been manufactured, which gives an injection distance of 9 mm. Before testing, we weighed and measured the length of each fuel grain.

DOI: 10.13009/EUCASS2022-4535

### 2.4 Test Procedure

To initiate the combustion, an electrically initiated igniter is used. Before the test, it is mounted to the face surface of the fuel grain using Kapton tape (Fig. 3). The pyrotechnic charge (COTS black powder with 20% nitrocellulose binder) has been minimized to not disrupt the fuel mass regression measurements, but still, allow for repeatable ignition. Then, fuel grain is installed in the thruster along with the nozzle and bulkhead endcaps. The igniter wires are connected to the electrical system, the feed system manual valves are open, and the test is ready to be initiated by the remote command.

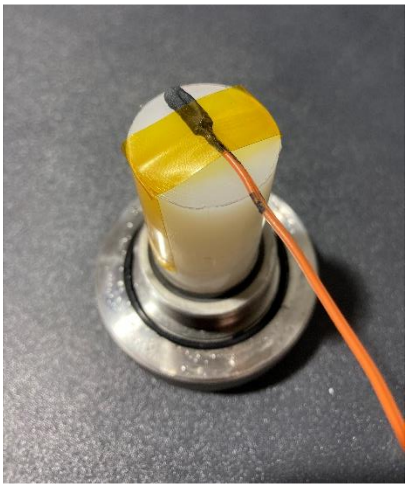

Figure 3. Fuel grain ready for testing: mounted on the bulkhead end cap with pyrotechnic igniter

The test sequence is automated and uses pre-defined open/close times for the main oxygen valve, purge valve, and igniter, to allow a repeatable testing procedure. Figure 4 below shows a typical test sequence. First, the oxygen valve is opened, then an igniter is fired to initiate the combustion. The 200 ms delay between oxygen valve and igniter has been set, as it allowed oxygen to fill the chamber and gave the most repeatable ignition. After the test, the purge valve is opened to remove the oxidizer from the feed system and stop the combustion.

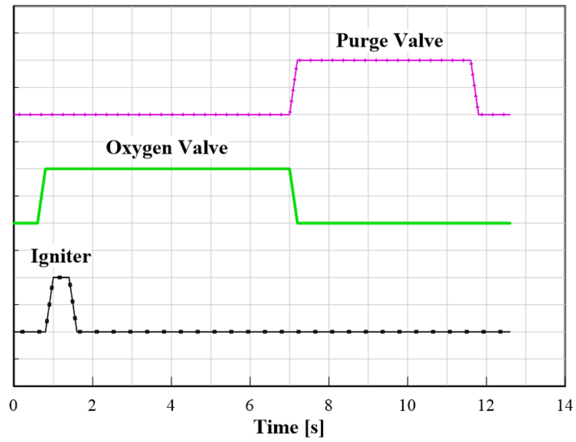


Figure 4. Typical test sequence for 6-second burn

## 2. Hot Fire Testing

Hot fire testing has been performed for 10 HDPE fuel grains to characterize the regression rate of the end-burning hybrid propellant thruster. The burn duration has been selected as the first experimental variable (3, 6, 9 seconds), as it is interesting to see the evolution of the fuel surface in time. The mass flow rate of the oxidizer is the second variable. Unfortunately, due to flowmeter malfunction, we were unable to measure the flow rate for these tests. It is controlled by the oxidizer pressure set on the outlet from the tank pressure regulator, so we used two pressure levels of 6 and 10 bar for these tests. As the oxidizer mass flux ($G_{ox}$) is the key variable in calculating the regression rate, we can only provide an estimated oxidizer mass flow rate for these two pressure levels. The test matrix is presented

DOI: 10.13009/EUCASS2022-4535



in Table 1. Each burn duration / pressure level has been performed twice, except for the longest burns, as they were limited by the nozzle insulation life.

Table 1: Test matrix

| Hot Fire Test No. | Burn duration [s] | Oxidizer pressure [bar] | Oxidizer mass flow rate [g/s] |
|---|---|---|---|
| 1 | 3 | 6 | 2.5 |
| 2 | 3 | 6 | 2.5 |
| 3 | 3 | 10 | 5.2 |
| 4 | 3 | 10 | 5.2 |
| 5 | 6 | 6 | 2.5 |
| 6 | 6 | 6 | 2.5 |
| 7 | 6 | 10 | 5.2 |
| 8 | 6 | 10 | 5.2 |
| 9 | 9 | 6 | 2.5 |
| 10 | 9 | 10 | 5.2 |

Figure 5 gives a typical combustion chamber pressure-time trace. It can be seen that pressure rises first due to the oxygen valve opening (point A), then igniter fires (point B). The delay between the command and igniter firing can reach up to several hundred milliseconds, which introduces variability in actual burn duration between tests. Immediately after igniter firing the pressure spike can be observed due to the fast combustion of the pyrotechnic charge in an oxygen-rich atmosphere, after which a relatively stable burn follows. At point D the oxygen valve is closed, and pressure drops sharply, but at the same time purge valve is opened and nitrogen reaches the combustion chamber raising the pressure for a brief moment. Figure 7 gives pressure-time history for all hot-fire tests, showing very good repeatability of the test sequence. Still, ignition delay times or pressure curves vary between tests with the same experimental conditions. An in-depth analysis of this behavior is beyond the scope of this paper, but obtained curves seem to be reasonably good to proceed with the analysis of the regression rate of the fuel.

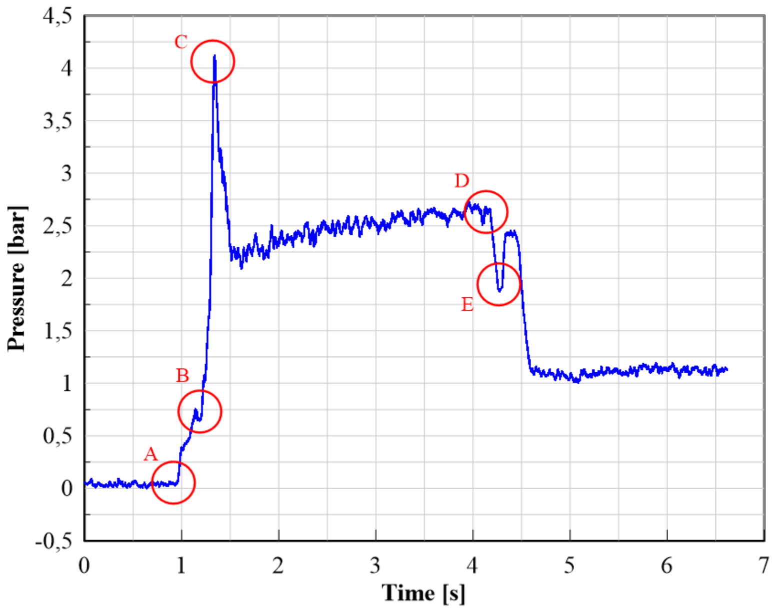


Figure 5. Combustion chamber pressure-time history for Hot Fire Test No. 4 showing typical events during the test sequence.

Figure 6. Photo of the Hot Fire Test No. 10 (ignition – left, stable burn – right).

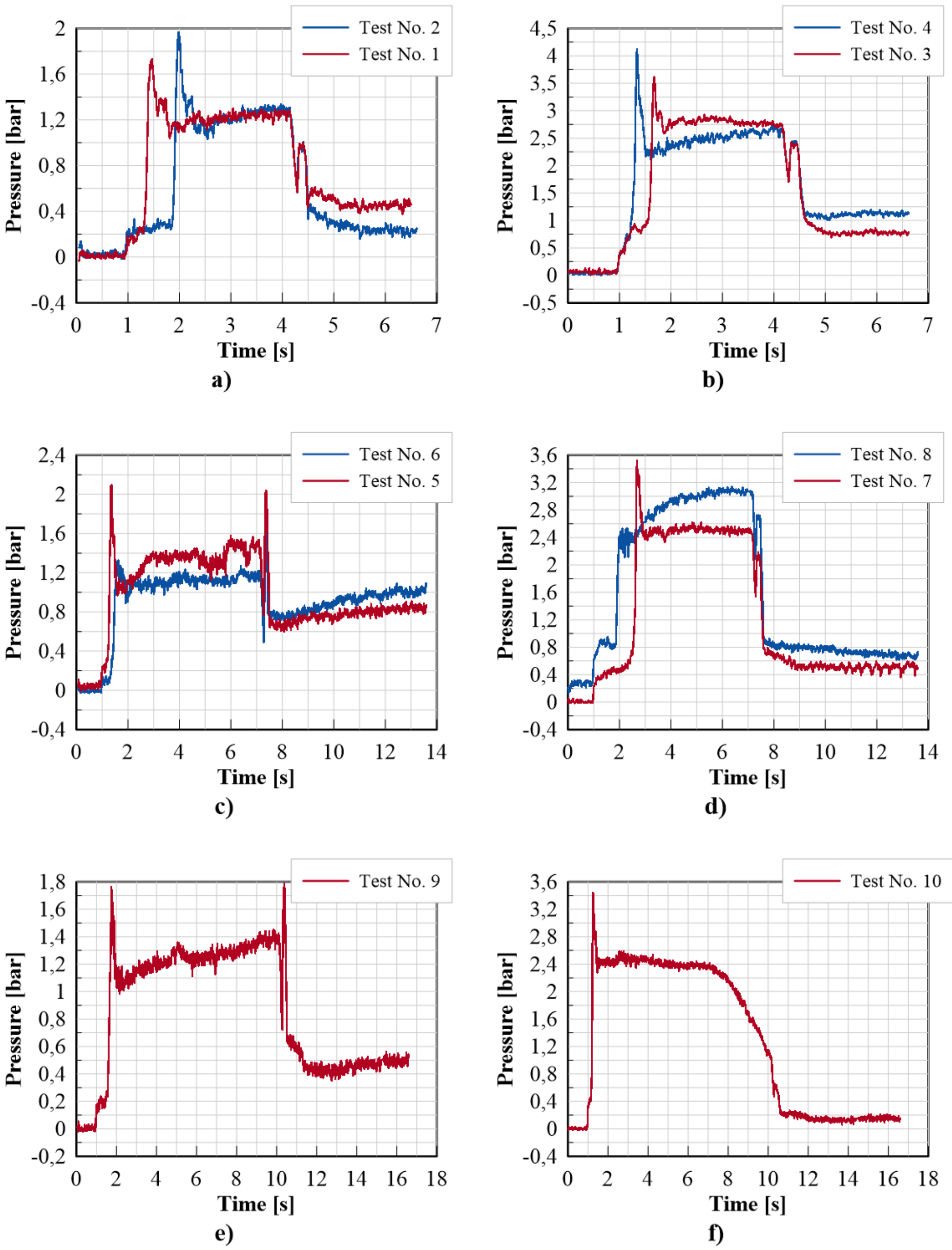


Figure 7. Combustion chamber pressure time history for all hot fire tests. Figures a), c), e) – 6 bar oxidizer pressure, b), d), f) – 10 bar oxidizer pressure.

DOI: 10.13009/EUCASS2022-4535



## 3. Results

### 4.1 Axial regression rate

After testing, each fuel grain has been carefully removed from the thruster, photographed, and weighted. Its face surface has been measured with a manual 2-axis measurement probe with a digital readout (accuracy ± 0.01 mm). The fuel grains' length before testing have been 39.82 mm ± 0.11, and the mass was 19.00 g ± 0.10. Table 2 gives actual burn duration (by the pressure curves), fuel grain mass after the test, and average axial regression rate calculated by loss in mass:

$$\dot{r}_x = \frac{\Delta m_f}{(\rho_f A_c t_b)}, \tag{2}$$

where $\Delta m_f$ - fuel mass loss, $\rho_f$ - fuel density, $A_c$ - the initial area of the fuel face surface, $t_b$ - actual burn time. Calculated average axial regression, based on the fuel mass loss, is plotted for each fuel in Figure 9. Tests with higher oxidizer pressure, thus higher oxidizer mass flow rate, achieved larger regression, which is well known and expected behavior. Interestingly, the data points seem to follow a linear trend with increasing burn duration. There are many factors suggesting that regression should increase or decrease in time. For example, during the burn, the injection distance increases as the fuel is consumed. Additionally, as can be seen in the next chapter, the fuel surface area evolves due to radial regression rate non-uniformities. However, obtained data is too scarce (too few tests, too short burn duration) to confirm linear relation.

Figure 8. Photo of the fuel grains for Tests No. 5, 7, 10 (from left to right), clearly showing the evolution of the face surface with increasing burn duration and total oxidizer mass throughput.

Table 2: Hot Fire Test results

| **Hot Fire Test No.** | **Actual burn duration [s]** | **Oxidizer pressure [bar]** | **Fuel grain mass after the test [g]** | **Average axial regression rate [mm/s]** |
|---|---|---|---|---|
| 1 | 2.97 | 6 | 18.29 | 0.55 |
| 2 | 2.38 | 6 | 18.48 | 0.47 |
| 3 | 2.73 | 10 | 18.06 | 0.83 |
| 4 | 3.00 | 10 | 17.87 | 0.64 |
| 5 | 5.85 | 6 | 17.46 | 0.57 |
| 6 | 5.76 | 6 | 17.51 | 0.60 |
| 7 | 4.60 | 10 | 17.38 | 0.76 |
| 8 | 5.31 | 10 | 17.00 | 0.82 |
| 9 | 8.56 | 6 | 16.98 | 0.53 |
| 10 | 9.00 | 10 | 15.82 | 0.75 |

DOI: 10.13009/EUCASS2022-4535

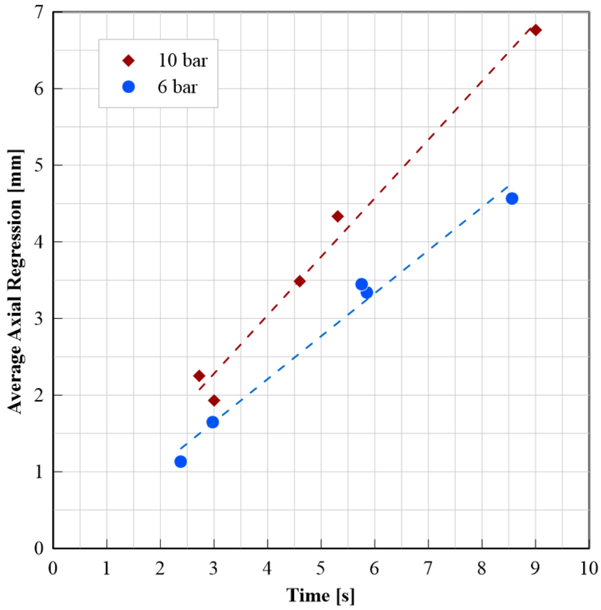


Figure 9. Average axial fuel regression for each test.

## 4.2 Radial regression rate

As can be seen from the photos in Figure 8, the fuel face surface becomes highly non-uniform with increasing burn duration and oxidizer mass flow rate. A clear vortex pattern is formed on the surface. To analyze the radial regression rate, the fuel grain length has been measured at different points. Based on those measurements and actual burn duration, a local regression rate for each point has been found. Figure 10 gives the distribution of the fuel regression rate along the radial direction for all measurements, along with the averaged regression rate at a single measurement point, for both oxidizer pressures.

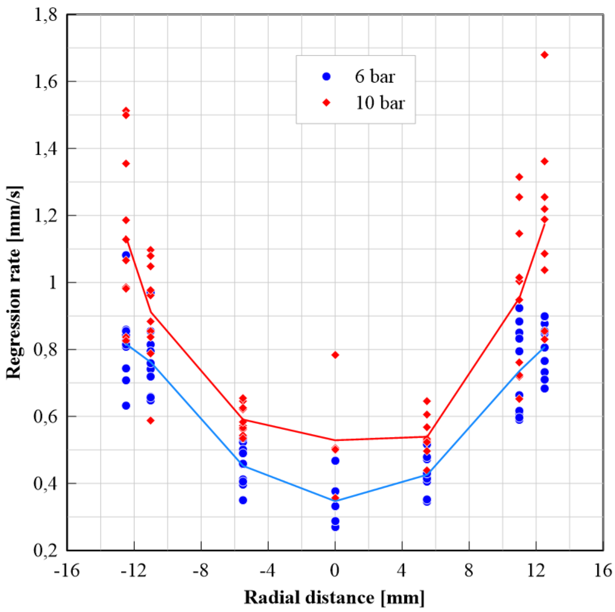


Figure 10. Fuel regression rate distribution along the radial direction.

The non-uniform radial regression rate has been observed in many studies before and it has been expected. However, the shape of the non-uniformity is entirely contrary to those reported by Rice et al. [15], Hayashi et al. [16], or Lestrade et al. [5]. In their studies, a depression formed at the center section of the fuel surface due to a higher regression rate, while in our case it is the opposite, namely, the regression rate is the highest in the outer edges of the fuel surface. The high non-uniformity and formed vortex pattern can be attributed to the low number of injectors (two) in our study, as other researchers used even six injectors to achieve a more uniform regression rate. However, several other differences may have an impact on this result such as chamber diameter, injection distance, oxidizer injector mass flux, combustion chamber length, and nozzle throat diameter. The detailed analysis of these variables is out of the scope of this paper, as it only presents preliminary data, and more testing is needed.

## 4. Conclusions

This paper presented the first results of the work being performed at the AGH University of Science and Technology, with a long-term goal to develop and demonstrate the feasibility of using a hybrid rocket engine as green, chemical propulsion for small satellites. For that purpose, a new test facility has been developed to perform a series of hot firings of different thruster test articles. The first test campaign was successful and provided valuable data on the regression rate of the 25 mm diameter, end-burning hybrid propellant thruster using GOX/HDPE. Unfortunately, due to flowmeter malfunction, the regression rate cannot be quantified in terms of oxidizer mass flux at this point, but this will be addressed in the next test campaign.

The obtained data give more evidence on the non-uniform regression rate behavior in end-burning hybrids. The most interesting result is that the non-uniformity shape achieved in this study is opposite to those reported by other researchers. However, more testing is needed with other design variables to explain this behavior.

## Acknowledgments

This project has been funded by the Faculty of Mechanical Engineering and Robotics at AGH University of Science and Technology and is conducted in collaboration with the Progresja Space company. The authors are grateful for this help.

## References

References must be numbered in the text in the following style [3] and listed at the end of the paper in the following way.

[1] K. Anflo and B. Crowe, "In-space demonstration of an ADN-based propulsion system," in *47th AIAA/ASME/SAE/ASEE Joint Propulsion Conference \& Exhibit*, 2011, p. 5832.

[2] R. K. Masse *et al.*, "AF-M315E Propulsion System Advances & Improvements," pp. 1–10, 2016, doi: 10.2514/6.2016-4577.

[3] S. A. Whitmore, "Nytrox as 'Drop-in' replacement for gaseous oxygen in smallsat hybrid propulsion systems," *Aerospace*, vol. 7, no. 4, 2020, doi: 10.3390/aerospace7040043.

[4] N. Pokrupa, K. Anflo, and O. Svensson, "Spacecraft system level design with regards to incorporation of a new green propulsion system," in *47th AIAA/ASME/SAE/ASEE Joint Propulsion Conference \& Exhibit*, 2011, p. 6129.

[5] J. Y. Lestrade, J. Messineo, J. Anthoine, A. Musker, and F. Barato, "Development and Test of an Innovative Hybrid Rocket Combustion Chamber," *7th Eur. Conf. Aeronaut. ans Sp. Sci.*, pp. 1–9, 2017, doi: 10.13009/EUCASS2017-414.

[6] F. Martin, "Promising Space Transportation Applications Using Hybrid Propulsion," no. July, pp. 25–28, 2010.

[7] E. T. Jens, A. C. Karp, B. Nakazono, D. Eldred, M. Devost, and D. Vaughan, "Design of a Hybrid CubeSat Orbit Insertion Motor," pp. 1–19, 2016, doi: 10.2514/6.2016-4961.

[8] E. E. Rice, M. J. Chiaverini, C. P. St. Clair, W. H. Knuth, and R. J. Gustafson, "Mars ISRU CO/O2 hybrid engine development status," *38th Aerosp. Sci. Meet. Exhib.*, no. c, 2000, doi: 10.2514/6.2000-1066.

[9] S. A. Whitmore, "Additively Manufactured Acrylonitrile-Butadiene-Styrene–Nitrous-Oxide Hybrid Rocket Motor with Electrostatic Igniter," *J. Propuls. Power*, vol. 31, no. 4, 2015, doi: 10.2514/1.B35681.

[10] S. D. Mathias, S. A. Whitmore, and R. Harvey, "High Voltage Breakdown and Arc-Tracking Mechanism of Thermoplastics with Applications to Hybrid Rocket Arc- Ignition," no. July, pp. 1–13, 2017, doi: 10.2514/6.2017-4601.

[11] E. T. Jens, A. C. Karp, J. Rabinovitch, B. Nakazono, A. Conte, and D. A. Vaughan, "Design of interplanetary hybrid cubesat and smallsat propulsion systems," *2018 Jt. Propuls. Conf.*, pp. 1–18, 2018, doi: 10.2514/6.2018-4668.

[12] E. T. Jens *et al.*, "Low pressure ignition testing of a hybrid smallsat motor," *AIAA Propuls. Energy Forum Expo. 2019*, no. August, 2019, doi: 10.2514/6.2019-4009.

[13] L. Simurda and G. Zilliac, "Continued testing of a high performance hybrid propulsion system for small

satellites," *51st AIAA/SAE/ASEE Jt. Propuls. Conf.*, pp. 1–23, 2015, doi: 10.2514/6.2015-4201.
[14] A. Karabeyoğlu, E. Toson, and B. Evans, "'O/F shift' in hybrid rockets," *50th AIAA/ASME/SAE/ASEE Jt. Propuls. Conf. 2014*, pp. 1–19, 2014, doi: 10.2514/6.2014-3851.
[15] E. E. Rice, D. J. Gramer, C. P. St. Clair, and Chiaver, "MARS ISRU CO/O2 ROCKET ENGINE DEVELOPMENT AND TESTING," in *Seventh International Workshop on Microgravity Combustion and Chemically Reacting Systems*, 2003, no. August.
[16] D. Hayashi and T. Sakurai, "A Fundamental Study of An End - Burning Swirling - Flow," in *51st AIAA/SAE/ASEE Joint Propulsion Conference*, 2015, pp. 1–8.
[17] E. P. Volchkov, S. V Semenov, and V. I. Terekhov, "Turbulent heat transfer at the forward face surface of a vortex chamber," *J. Eng. Phys.*, vol. 56, no. 2, pp. 109–115, 1989.
[18] C. Paravan, F. Piscaglia, and L. Galfetti, "Influence of Operating Parameters on the Ballistics of a Lab-Scale Vortex Flow Pancake Hybrid Rocket Engine," pp. 1–9, 2015.
[19] C. Paravan, J. Glowacki, S. Carlotti, F. Maggi, and L. Galfetti, "Vortex combustion in a hybrid rocket motor," *52nd AIAA/SAE/ASEE Jt. Propuls. Conf. 2016*, pp. 1–21, 2016, doi: 10.2514/6.2016-4562.
[20] J. Glowacki, F. Maggi, and L. Galfetti, "Numerical Simulation of Vortex Combustion in a Hybrid Rocket Motor," *7Th Eur. Conf. Aeronaut. Aerosp. Sci.*, 2017, doi: 10.13009/EUCASS2017-477.
[21] J. Y. Lestrade, J. Anthoine, A. J. Musker, and A. Lecossais, "Experimental demonstration of an end-burning swirling flow hybrid rocket engine," *Aerosp. Sci. Technol.*, vol. 92, pp. 1–8, 2019, doi: 10.1016/j.ast.2019.05.057.